# Direct detection of sub-GeV dark matter with scintillating targets

Stephen Derenzo,[1,*] Rouven Essig,[2,†] Andrea Massari,[2,‡] Adrián Soto,[3,4,§] and Tien-Tien Yu[2,‖]

[1]*Lawrence Berkeley National Laboratory, Mail Stop 55-121, Berkeley, California 94720, USA*
[2]*C.N. Yang Institute for Theoretical Physics, Stony Brook University, Stony Brook, New York 11794, USA*
[3]*Department of Physics and Astronomy, Stony Brook University, Stony Brook, New York 11794-3800, USA*
[4]*Institute for Advanced Computational Science, Stony Brook University, Stony Brook, New York 11794, USA*

(Received 7 July 2016; revised manuscript received 24 October 2016; published 28 July 2017)

We suggest a novel experimental concept for detecting MeV-to-GeV-mass dark matter, in which the dark matter scatters off electrons in a scintillating target and produces a signal of one or a few photons. New large-area photodetectors are needed to measure the photon signal with negligible dark counts, which could be constructed from transition edge sensor (TES) or microwave kinetic inductance detector (MKID) technology. Alternatively, detecting two photons in coincidence may allow the use of conventional photodetectors like photomultiplier tubes. We describe why scintillators may have distinct advantages over other experiments searching for a low ionization signal from sub-GeV dark matter, as there are fewer potential sources of spurious backgrounds. We discuss various target choices, but focus on calculating the expected dark matter-electron scattering rates in three scintillating crystals: sodium iodide (NaI), cesium iodide (CsI), and gallium arsenide (GaAs). Among these, GaAs has the lowest band gap (1.52 eV) compared to NaI (5.9 eV) or CsI (6.4 eV), which in principle allows it to probe dark matter masses as low as ∼0.5 MeV, compared to ∼1.5 MeV with NaI or CsI. We compare these scattering rates with those expected in silicon (Si) and germanium (Ge). The proposed experimental concept presents an important complementary path to existing efforts, and its potential advantages may make it the most sensitive direct-detection probe of dark matter down to MeV masses.

DOI: 10.1103/PhysRevD.96.016026

## I. INTRODUCTION

Dark matter (DM) with a mass in the MeV–GeV range is phenomenologically viable and has received increasing attention in recent years [1–8]. An important probe for DM is with *direct detection* experiments, in which a DM particle in the Milky-Way halo interacts with some target material in a detector, producing an observable signal in the form of heat, phonons, electrons, or photons [9]. The traditional technique of searching for nuclear recoils loses sensitivity rapidly for DM masses below a few GeV, since the DM is unable to transfer enough of its energy to the nucleus, resulting in no observable signal above detector thresholds. However, DM scattering off electrons, whose mass is much less than a nucleus, can lead to observable signals for masses well below 1 GeV [1], opening up vast new regions of parameter space for experimental exploration.

DM-electron scattering in direct detection experiments has been investigated for noble liquid targets [1,5] and was demonstrated explicitly to have sensitivity down to DM masses of a few MeV and cross sections of $\sim 10^{-37}$ cm$^2$ [5] using published XENON10 data [10]. Future improvements using xenon-based detectors depend on whether a spurious background of electrons can be reduced. Several other ideas have been suggested to improve the cross-section sensitivity and lower the mass threshold. Semiconductor targets like silicon (Si) and germanium (Ge), as used by e.g. SuperCDMS [11] and DAMIC [12], could provide sensitive probes for masses as low as a few hundred keV [1–4]. Two-dimensional targets, like graphene, could probe a directional signal for DM masses above a few MeV [6], and superconductors or superfluids may probe masses well below 1 MeV [6]. These ideas still require further R&D and explicit demonstration, motivating the exploration of alternate approaches.

In this paper, we explore using a *scintillator* as the target material to search for DM with masses as low as a few hundred keV. One or more scintillation photons are emitted when an electron excited by a DM-electron scattering interaction relaxes to the ground state. Several possible scintillating materials exist. In this paper, we focus on three crystals: sodium iodide (NaI), cesium iodide (CsI), and gallium arsenide (GaAs). Other materials will be mentioned briefly.

The outline of the paper is as follows. Section II describes the basic detection idea. Section III discusses the specific advantages and challenges of using scintillating crystals to detect sub-GeV DM. We also discuss possible backgrounds and compare the use of scintillators to other approaches. In Sec. IV, we describe our calculations and summarize the physics of DM scattering off electrons.

*sederenzo@lbl.gov
†rouven.essig@stonybrook.edu
‡andrea.massari@stonybrook.edu
§adrian.soto-cambres@stonybrook.edu
‖chiu-tien.yu@stonybrook.edu

 

Section V summarizes the properties of the scintillating targets. Section VI describes the numerical calculations, and Sec. VII presents our results. Several appendices provide additional details, including a discussion of other possible scintillating targets, a review of the scintillation mechanism, and the effect of excitons on the DM-electron scattering-rate calculation. We also give the electron recoil spectra in GaAs, NaI, and CsI, as well as the density of states and band structures.

## II. BASIC DETECTION IDEA

The basic detection idea is shown in Fig. 1. A dark-matter particle scatters off an electron in the valence band of a crystal, promoting the electron to the conduction band and creating an electron-hole pair [1].[1] The typical energy transfer from the $\mathcal{O}(\mathrm{MeV})$ DM particle to the electron is a few eV (see below and [2]), but higher energy transfers are possible with a suppressed cross section. If the initial electron-recoil energy is sufficiently large, additional electron-hole pairs may be created as the electron quickly relaxes to the bottom of the conduction band. In a scintillator, the electron-hole pairs can then recombine or the electron or hole can get captured by radiative centers (created by, for example, doping the target material with a suitable element), which produces one or more photons. In a scintillator with high radiative efficiency, the number of photons corresponds to the number of electron-hole pairs. These photons then escape the target material and are detected with photodetectors that surround the target material.

The target and detector array need to be at low (e.g., cryogenic) temperatures to avoid excitations induced by thermal fluctuations. An active shield surrounds the detector to veto radioactive backgrounds, including gamma rays that Compton-scatter in the target material. An optical filter between the scintillator and the photodetector could ensure passage of only the expected photon wavelengths, which would remove some possible background events.

To detect a single photon in a rare event search, new photodetectors with low dark counts are needed. Detectors with single-photon sensitivity and no dark counts exist, e.g. MKIDs [14] and TESs [15], which operate at cryogenic temperatures of $\mathcal{O}(100\ \mathrm{mK})$ and have sub-eV energy resolution and microsecond time response [14]. MKIDs (TESs) have demonstrated single-photon sensitivity at photon energies of ∼0.25–12.4 eV [14] (∼0.04–3.1 eV [16]), with the potential to be sensitive to meV phonon energies [6,17]. However, currently the most sensitive single-photon devices [6,18–20] are small in size, $\sim((5\text{–}125)\ \mu\mathrm{m})^3$, and R&D is required to build a 10–100 $\mathrm{cm}^2$ photodetector capable of covering a $\mathcal{O}(1\ \mathrm{kg})$ target. Collaborators on

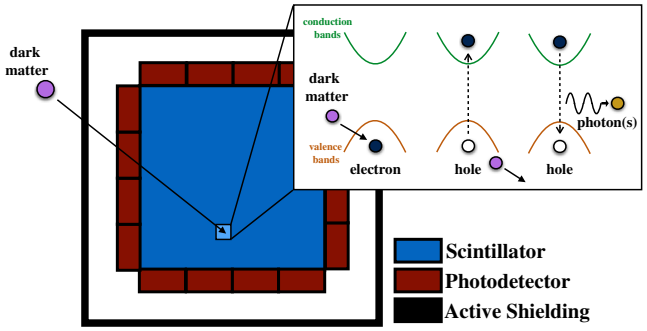


FIG. 1. Schematic experimental concept: a DM particle scatters off an electron in the valence band of a scintillating crystal target, exciting it to a higher-energy level; one or more scintillation photons from the relaxation of the electron to the ground state are observed by a surrounding photodetector array. The detector is encased in an active shield to eliminate environmental backgrounds. Compared to other approaches that attempt to measure the charge directly (in e.g. semiconductor targets), here no electric field is needed, reducing or eliminating many potential detector-specific backgrounds.

CRESST-II, focused on DM-nucleus scattering, have already developed an $\mathcal{O}(10\ \mathrm{cm}^2)$ photodetector sensitive to $\mathcal{O}(10)$ photons using a TES read out by SQUIDs [21,22]. SuperCDMS TES phonon-detector technology is also being repurposed to serve as a photodetector [23].[2] Our work further motivates this R&D, and emphasizes that such detectors could probe three orders of magnitude lower in DM mass than the standard DM-nucleus recoil searches.

Alternatively, more conventional photodetectors (like photomultiplier tubes) could be used to search for two photons in coincidence (see e.g. [26]). This would necessitate that the electron struck by the DM receives a somewhat higher recoil energy, so that it can create two electron-hole pairs, each of which produce one photon. This would lead to a somewhat higher DM-mass threshold, but in low band-gap materials like GaAs, the two-photon DM-scattering event rate is comparable to the one-photon rate as we will show with our calculation below.

## III. SCINTILLATORS: ADVANTAGES AND CHALLENGES COMPARED TO OTHER APPROACHES

Several signals are possible when sub-GeV DM scatters off a bound electron in an atom or a crystal, exciting the electron to a higher energy level or an unbound state [1]. Depending on the target material, an experiment can either attempt to measure an ionization signal, which is obtained by manipulating the electron with an electric field, or measure one or more scintillation photons, which are

[1]Note that [13] proposed the search of one or more photons from weak-scale DM through atomic excitations.

[2]Silicon photomultipliers (SiPM) are possible photodetectors and operate well at cryogenic temperatures, but the dark-count rate may be too large [24,25].

emitted as the electron relaxes back to its ground state. Until now, the latter approach has not been considered in detail.

Measuring the ionization signal has already constrained DM as light as a few MeV [5], using XENON10's two-phase xenon time projection chamber (TPC). Unfortunately, several possible spurious backgrounds exist, so one cannot currently claim that the observed one- and few-electron events are from DM [5,10,27]. Using semiconductors, CDMSlite [11] applied a bias voltage, forcing a conduction-band electron to traverse the material and generate enough Neganov-Luke phonons [28,29] to be measured by phonon detectors. The CDMSlite setup with improved phonon detectors may in the future surpass xenon-based TPCs in their sensitivity to sub-GeV DM. However, while there may be fewer dark counts than for two-phase xenon TPCs, the presence of an electric field may create spontaneous electron-hole pairs that could mimic a DM signal. Therefore, more work is needed to establish the potential of the CDMSlite setup.

Traditional direct-detection experiments search for WIMP-induced nuclear recoils with recoil energies of order a few keV. Backgrounds to these searches include Compton scattering and beta decays, which dominate at energies of order a few keV. Experiments searching for WIMPs are usually sensitive to a combination of scintillation, ionization, and phonon signals, allowing nuclear recoils (produced by a WIMP) to be discriminated from electron recoils (produced by Compton scattering and beta decays). In contrast to WIMP searches, DM scattering off electrons produces the same "signal" as Compton scattering and beta decays. However, as we will discuss in Sec. IV, the typical electron-recoil energy from sub-GeV DM-electron scattering is a few eV, well below the typical energies of the background events. The background event rate is much lower in the few-eV energy range.

While radioactive backgrounds have been measured only at slightly higher energies than those of interest, they are expected to be flat down to lower energies. The SuperCDMS collaboration has measured their backgrounds down to about 56 eV in their CDMSlite run, finding a rate of about 0.4 events/kg/year/eV [11]. They have also calculated the expected backgrounds down to 40 eV for their silicon and germanium detectors in the upcoming experiment at SNOLAB, and expect on average a background of about 0.027 (0.3) events/kg/year/eV in germanium (silicon), see Table V in [30]. At slightly higher energies, SABRE will use NaI(Tl) and expects a background of below 0.1 events/kg/year/eV [31]. The KIMS collaboration, using CsI(Tl), measured a background of $< 1$ event/kg/year/eV [32]. The Majorana Demonstrator experiment measured a background of 0.04 events/kg/year/eV [33]. This shows that experiments regularly are able to shield their detector and purify materials sufficiently to have a low background rate. Among the materials studied in this paper (NaI, CsI, and GaAs), GaAs has not been used previously in a dark matter experiment, but GaAs is not known to have any radioactive impurities that would produce a larger background rate. Very few background events are thus expected in the few-eV energy range for an exposure of $< 1$ kg-year. This is sufficient to probe orders of magnitude of unexplored DM parameter space.[3]

Instead of radioactive backgrounds discussed above, a far greater background challenge is to control "dark counts", which we here take to be any detector specific backgrounds. A striking example of this is the XENON10 data mentioned above [10]. While it led to the first limit on sub-GeV DM, this data contains a large number of background events. The events likely have several origins, including for example electrons, created by highly-ionizing background events, that get trapped at the liquid-gas interface and are spontaneously emitted hundreds of milliseconds later. Other detector setups may suffer from other dark counts. Moreover, whenever an electric field is required to amplify a signal, dark counts (from, e.g., leakage currents) may be a source of backgrounds.

A potential background for scintillators is phosphorescence induced from a previous interaction (afterglow). Our candidate targets scintillate on nano-to-millisecond timescales, but some photons could arise from excited states whose lifetimes are much longer (phosphorescent) due to a "forbidden" radiative transition. The phosphorescent photons typically have a lower energy, so if the photodetector cannot reject them using pulse height, a narrow-band optical filter could be placed between scintillator and photodetector to remove phosphorescent photons.

Leakage currents are the limiting factor to the sensitivity of semiconductor targets for low mass DM while afterglow may be a limiting factor for scintillating targets. Neither leakage currents nor afterglow are well-studied at cryogenic temperatures. Therefore, it is important to explore both semiconductor and scintillating targets. One argument in favor of GaAs as a donor-acceptor scintillator is that GaAs crystals doped at the Mott limit will have no afterglow because the free carriers that fill the crystal will efficiently annihilate any metastable radiative states.

We note that a few handles exist to distinguish a DM signal from a background. First, the signal rate modulates annually and daily due to the motion of the Earth [34]. The modulation is larger than for elastic WIMP-nucleus recoils, since the scattering is inelastic [35], and increases with threshold (see discussion in Sec. IV). Backgrounds are not expected to have the same phase, amplitude, period, and energy dependence. Second, the DM-induced electron-recoil spectrum is distinctive and unlikely to be mimicked by a background. Third, the DM signal scales with the target volume, in contrast to many potential backgrounds

[3]We note that solar neutrinos will also not contribute for exposures $\lesssim 1$ kg-year [1].

arising from the surrounding detector package. This can be confirmed by using the same detector but with a hollow crystal.[4] Backgrounds that scale with the target volume, such as external gammas and phosphorescence, can be determined by measuring the change in signal when a gamma ray source is placed outside the detector.

## IV. DARK MATTER-ELECTRON SCATTERING

To explain our choice of scintillating materials, we review here the scattering of sub-GeV DM off a bound electron in a crystal. The salient features emphasized below also apply to atoms. See [2] for details.

The rate for DM-electron scattering to excite an electron from level $i$ to $f$ is

$$\frac{dR_{\rm crystal}}{d\ln E_e} = \frac{\rho_\chi}{m_\chi} N_{\rm cell} \bar{\sigma}_e \alpha \frac{m_e^2}{\mu_{\chi e}^2} \times \int d\ln q \left( \frac{E_e}{q} \eta(v_{\rm min}(q, E_e)) \right) \times |F_{\rm DM}(q)|^2 |f_{\rm crystal}(q, E_e)|^2, \quad (1)$$

where $\alpha \simeq 1/137$ is the fine-structure constant, $m_\chi$ ($m_e$) denotes the DM (electron) mass, $\rho_\chi \simeq 0.4$ GeV/cm$^3$ is the local DM density, $E_e$ is the total energy deposited, $q$ is the DM-to-electron momentum transfer, $N_{\rm cell} = M_{\rm target}/M_{\rm cell}$ is the number of unit cells in the target crystal of total (cell) mass $M_{\rm target}$ ($M_{\rm cell}$), and $\mu_{\chi e}$ is the DM-electron reduced mass. The *crystal form-factor* is

$$|f_{\rm crystal}(q, E_e)|^2 = \frac{2\pi^2 V_{\rm cell}}{\alpha m_e^2} \sum_{if} \int_{\rm BZ} \frac{d^3k d^3k'}{(2\pi)^6} \delta(E_e - \Delta E) \times \sum_{\boldsymbol{G}'} q \delta(q - |\boldsymbol{k}' - \boldsymbol{k} + \boldsymbol{G}'|) |f_{[i\boldsymbol{k}, f\boldsymbol{k}', \boldsymbol{G}']}|^2, \quad (2)$$

where $\Delta E = E_{f\boldsymbol{k}'} - E_{i\boldsymbol{k}}$, $V_{\rm cell}$ is the volume of the unit cell, $\boldsymbol{k}, \boldsymbol{k}'$ are wave vectors in the first Brillouin Zone (BZ), and $\boldsymbol{G}'$ is the reciprocal lattice vector. The reference cross-section $\bar{\sigma}_e$ and DM form factor $|F_{\rm DM}(q)|^2$ are parametrizations of the DM-electron interaction defined as

$$\overline{|\mathcal{M}_{\rm free}(\boldsymbol{q})|^2} \equiv \overline{|\mathcal{M}_{\rm free}(\alpha m_e)|^2} \times |F_{\rm DM}(q)|^2 \quad (3)$$

$$\bar{\sigma}_e \equiv \frac{\mu_{\chi e}^2 \overline{|\mathcal{M}_{\rm free}(\alpha m_e)|^2}}{16\pi m_\chi^2 m_e^2}, \quad (4)$$

where $\overline{|\mathcal{M}_{\rm free}|^2}$ is the absolute value squared of the elastic DM-free-electron scattering matrix element, averaged over initial-, and summed over final-state particle spins. $F_{\rm DM}$ captures the momentum-dependence of the DM scattering off a free electron; for example, if the particle mediating the DM-electron interaction is a vector boson whose mass is larger than the momentum transfer, $F_{\rm DM} = 1$, while if its mass is much less than the momentum transfer, then $F_{\rm DM} = (\alpha m_e/q)^2$ (other form factors are possible too) [1]. The DM-halo profile is

$$\eta(v_{\rm min}) = \int d^3 v_\chi g_\chi(\boldsymbol{v}_\chi) \frac{1}{v_\chi} \Theta(v_\chi - v_{\rm min}) \quad (5)$$

$$= \frac{1}{K} \int d\Omega dv_\chi v_\chi e^{-|\boldsymbol{v}_\chi - \boldsymbol{v}_{\rm E}|^2/v_0^2} \times \Theta(v_\chi - v_{\rm min}) \Theta(v_{\rm esc} - v_\chi), \quad (6)$$

where in Eq. (5) we chose for $g_\chi(\boldsymbol{v}_\chi)$ the standard Maxwell-Boltzmann distribution with a sharp cutoff. We take $v_0 = 230$ km/s, the Earth velocity about the galactic center $\boldsymbol{v}_{\rm E} = 240$ km/s, and the DM escape velocity from the galaxy as $v_{\rm esc} = 600$ km/s. $K = 6.75 \times 10^{22}$ (cm/s)$^3$ is the normalization factor. The minimum velocity required for scattering is

$$v_{\rm min}(q, E_e) = \frac{E_e}{q} + \frac{q}{2m_\chi}. \quad (7)$$

There are four salient features worth emphasizing for sub-GeV DM scattering off electrons:

(i) First, since the bound electron's momentum can be arbitrarily high (albeit with suppressed probability), $q$ can be arbitrarily high, so that in principle all of the DM's kinetic energy can be transferred to the electron (in sub-GeV DM scattering off nuclei only a fraction is transferred to a much heavier nucleus). Thus, $E_\chi = \frac{1}{2} m_\chi v_\chi^2 \geq E_e$ implies $m_\chi \gtrsim 250$ keV $\times (E_e/1\ {\rm eV})$ for $v_\chi \lesssim v_{\rm esc} + v_{\rm E}$. Therefore, smaller ionization energies or band gaps can probe lower DM masses, with crystal targets being sensitive down to masses of a few hundred keV.

(ii) Second, since the electron moves at a speed of $\sim\alpha$, much faster than the DM ($\sim 10^{-3}$), the electron determines the typical $q$, $q_{\rm typ}$. A rough estimate for $q_{\rm typ}$ is the crystal momentum, $2\pi/a \sim 2.3$ keV, where $a \sim 10\alpha m_e$ is the lattice constant for our target choices (see below). Since $E_e \sim \boldsymbol{q} \cdot \boldsymbol{v}_\chi$, the minimum $q$ to obtain a particular $E_e$ is given by $q \gtrsim q_{\rm typ} \times E_e/(2.3\ {\rm eV})$. A similar estimate holds for atoms [2]. The signal rate is thus larger in semiconductors with low band gaps ($\Delta E \sim 1$–$2$ eV) than insulators ($\Delta E \gtrsim 5$ eV) or noble liquids ($\Delta E \sim 12$, 16, 25 eV for xenon, argon, helium, respectively).

(iii) Third, while the value of $q$ is naturally $q_{\rm typ}$, $q$ can in fact be much larger as mentioned above. This allows

[4]We acknowledge Matthew Pyle for insightful discussions.

for much larger momentum transfers and recoil energies, although these are strongly suppressed.

(iv) Fourth, since the scattering is inelastic, the annual modulation of the signal rate is larger than for typical WIMP elastic scattering [35]. The energy transfer is given by $E_e = E_B + E_r$, where $E_B$ is the binding energy and $E_r$ is the energy of the recoiling electron. For an elastic scattering, $E_B = 0$, while for inelastic scattering $E_B > 0$. Therefore, for a fixed $E_r$, $E_e^{\text{elastic}} < E_e^{\text{inelastic}}$. Equation (7) shows that an increase in $E_e$ corresponds to an increase in $v_{\text{min}}$, and therefore the population of the sampled $v_{\text{DM}}$ increasingly comes from the tails of the velocity distribution. As a result, the relative change in the velocity of the DM in June and Dec is larger for inelastic scattering than for elastic.

## V. SCINTILLATING TARGETS

The previous discussion suggests using scintillating crystals with low band gaps. However, the crystals must also have high purity, high radiative efficiency (i.e. little nonradiative recombination of excited electron-hole pairs), and few native defects, all while being grown to large sizes ($\gtrsim$1 kg). We thus focus on NaI and CsI, but include GaAs, which may also satisfy these criteria. Table I (top) lists salient features.

NaI and CsI are insulators that scintillate efficiently through the decay of self-trapped excitons. They are used extensively due to their high light output and ease of production [37,40–46]. Pure CsI is being considered for a DM-nucleus-recoil search [22]. Early measurements of GaAs, a direct-gap semiconductor, showed a radiative efficiency (internal) of ~0.6 at 77 K when doped with donors or acceptors [39]. Conventional coupling to photodetectors is inefficient due to the high refractive index (~3.8) but one could apply photonic antireflective coatings or deposit the photodetectors directly onto the surfaces of the GaAs crystal to reduce internal reflection [47].

In addition to GaAs, other suitable low band gap materials may exist. Crystals with band gaps $\lesssim$few eV are likely semiconductors [48]. Among these, direct-gap semiconductors have a high radiative efficiency, but no obvious candidates exist that can be grown in large sizes besides GaAs. Indirect-gap semiconductors are more common, but their scintillation is slow and inefficient without doping. However, luminescence has been reported from doped Si [49,50] and Ge [51] at cryogenic temperatures (Table I, bottom). More research could reveal suitable dopants to achieve high radiative efficiency. We show results for Ge and Si below since they are potential scintillators and are also used in current experiments sensitive to an ionization signal (e.g. SuperCDMS, DAMIC).

Other scintillator targets are possible. We mention some other potential targets and review the scintillation mechanisms of the substances in Table I in the appendices.

TABLE I. Band gap ($E_g$), radiative efficiency, photon emission energy peak ($E_{\text{em}}^{\text{max}}$), radiative recombination time ($\tau$), and scintillation mechanism (SX = self-trapped excitons, BE = bound excitons) for candidate scintillators. We focus on (top table): pure NaI, pure CsI, and GaAs (doped with acceptors or donors). Si and Ge (bottom table) are used for comparison, and suitable dopants could allow them to scintillate.

| Material | $E_g$ [eV] | Rad. Eff. | $E_{\text{em}}^{\text{max}}$ [eV] | $\tau$ [ns] | Mechanism |
|---|---|---|---|---|---|
| NaI [36] | 5.9 | ~1 | 4.1 | 300 | SX |
| CsI [37,38] | 6.4 | ~1 | 4.0 | $10^3$ | SX |
| GaAs [39] | 1.52 | ~0.6 | ~1.5 | $10^{3a}$ | BE |

| Material | $E_g$ [eV] |
|---|---|
| Si | 0.67 |
| Ge | 1.1 |

[a]Expected (no measurement).

## VI. CALCULATIONS

We calculate the DM-electron scattering rates in NaI, CsI, and GaAs using the `QEdark` module developed in [2]. We use Perdew-Burke-Ernzerhof (PBE) functionals [52], norm-conserving pseudopotentials [53], and adjust the band gaps to the values in Table I using a scissor correction [54,55]. Table II lists the required calculation parameters. We include in the density functional theory (DFT) calculation all electrons with binding energies $E_B$ as low as the $3d$-shell of Ga (binding energy $E_B \sim 32$ eV), the $5p$- and $5s$-shell electrons ($E_B \sim 13$ eV and ~23 eV, respectively) of Cs, and the $3d$-shell electrons of Ge as in [2,4] (deeper electrons are irrelevant). The numerical uncertainty is estimated by choosing 30 random $k$-point meshes. The sensitivity lines for Ge and Si are from [2] (only one mesh is shown, but the uncertainty is small [2]).

Our calculations do not include exciton effects. In the appendices, we argue that exciton effects are negligible for the low-gap materials GaAs, Ge, or Si, and may have an $\mathcal{O}(1)$ effect on the scattering rates for NaI and CsI.

TABLE II. Computational parameters for various materials. Lattice constant ($a$), cell volume ($V_{\text{cell}}$), number of valence + conduction bands ($N_{\text{bands}}$), number of valence $v$ and core $c$ electrons ($N_e$), and number of runs with independent random $k$-point meshes times number of $k$-points in each mesh ($N_k$). Note that there are two atoms per unit cell.

| | $a$ (bohr) | $V_{\text{cell}}$ (bohr$^3$) | $N_{\text{bands}}$ | $N_e$ | $N_k$ |
|---|---|---|---|---|---|
| CsI | 8.6868 | 655.51 | 80 | $8_v + 8_{c,\text{Cs}}$ | $30 \times 125$ |
| NaI | 12.927 | 464.88 | 50 | $8_v$ | $30 \times 216$ |
| GaAs | 10.8690 | 321.00 | 60 | $8_v + 10_{c,\text{Ga}}$ | $30 \times 216$ |
| Ge | 10.8171 | 316.4269 | 66 | $8_v + 20_c$ | $1 \times 243$ |
| Si | 10.3305 | 275.6154 | 56 | $8_v$ | $1 \times 243$ |

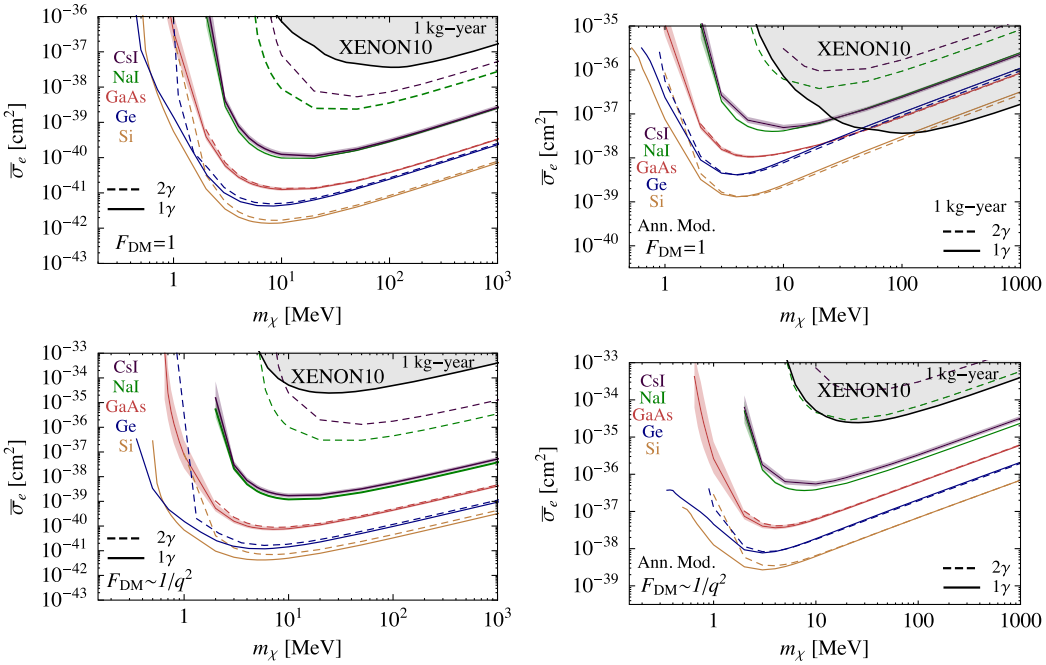


FIG. 2. DM-electron-scattering-cross-section ($\bar{\sigma}_e$) versus DM mass ($m_\chi$) for $F_{\rm DM}(q) = 1$ (top) and $F_{\rm DM}(q) = 1/q^2$ (bottom), assuming an exposure of 1 kg for 1 year and a radiative efficiency of 1. Left: Solid (dashed) lines show 3 events for a threshold of one (two) photons in CsI (purple), NaI (green), and GaAs (red). Bands around solid lines show the numerical uncertainty. Solid (dashed) lines for Ge (blue) and Si (gold) are the one(two)-electron threshold lines from [2]. Right: Solid (dashed) lines show $5\sigma$-discovery reach using annual modulation for a threshold of one (two) photons. The gray region is excluded by XENON10 [5].

## VII. RESULTS

Figure 2 (left) shows the potential sensitivity to $\bar{\sigma}_e$ [Eq. (3)] for two different $F_{\rm DM}$ [Eq. (4)], various materials, two thresholds, and data taken over one year with 1 kg of material. We assume a radiative efficiency of 1. The low-gap materials GaAs, Si, and Ge can reach potentially DM masses as low as a few hundred keV, whereas the reach of NaI and CsI is 1–2 MeV. This could probe lower masses than XENON10 [5], and extend the high-mass reach by one to several orders of magnitude.

The signal in GaAs, NaI, and CsI consists of one or more photons, while in Ge and Si it consists of either one or more electrons, or (if suitable dopants can provide a high radiative efficiency) one or more photons. We show two thresholds: "$1\gamma$" requires $E_e \geq E_g$, while "$2\gamma$" requires $E_e \geq E_g + \langle E \rangle$, where $\langle E \rangle$ is the mean energy needed for the recoiling electron to form another electron-hole pair. A phenomenological approach gives $\langle E \rangle \sim 2.9$ eV (3.6 eV, 4.2 eV) for Ge (Si, GaAs) [2,56,57]. Precise values for CsI and NaI are unavailable, so we show $\langle E \rangle = 3E_g$ [57]. More theoretical work and an experimental calibration can better quantify the number of photons produced by low-energy electron recoils. The mass threshold is different for the $1\gamma$ and $2\gamma$ lines. However, the low-gap materials have a similar high-mass reach for either threshold, since $E_e$ is typically several eV and more likely to produce two rather than one photon. Resolving two photons in coincidence can help reduce backgrounds.

The annual modulation of the signal rate can be used as a discriminant from background [34]. Figure 2 (right) shows $5\sigma$ discovery lines for which $\Delta S/\sqrt{S_{\rm tot} + B} = 5$ with $B = 0$. Here $\Delta S$ is the modulation amplitude and $S_{\rm tot}$ ($B$) is the total number of signal (background) events. The sensitivity weakens $\propto \sqrt{B}$, assuming $B$ is constant in time.

To summarize, we described a novel search for sub-GeV DM, using scintillators. Scintillators provide a complementary path with potential advantages over other approaches searching for a low ionization signal: the detection of photons may be technologically easier with fewer dark counts.

## ACKNOWLEDGMENTS

We are grateful to Matthew Pyle for numerous insightful discussions, including discussing potential backgrounds (like afterglow), and for suggesting how these could be characterized. We are also grateful to Jeremy Mardon and Tomer Volansky for numerous stimulating conversations. We thank Philip Allen, Jeremy Mardon, and Matthew Pyle for comments on a draft of this manuscript. We have benefited from many useful conversations with Thomas Allison, Mariví Fernández-Serra, Eden Figueroa, Enectali

Figueroa-Feliciano, Lauren Hsu, Mark Hybertsen, Serge Luryi, Aaron Manalaysay, Ben Mazin, Daniel McKinsey, Laszlo Mihaly, Florian Reindl, Karoline Schäffner, and Craig Woody. R. E. is supported by the DoE Early Career research program DESC0008061 and through a Sloan Foundation Research Fellowship. T.-T. Y. is also supported by Grant No. DESC0008061. A. M. acknowledges support from NSF grant PHY1316617. A. S. acknowledges support from DoE Grant No. DE-FG02-09ER16052. S. D. acknowledges support from the U.S. Department of Homeland Security, Domestic Nuclear Detection Office. This research used resources of the National Energy Research Scientific Computing Center, a DoE Office of Science User Facility supported by the Office of Science of the U.S. Department of Energy under Contract No. DE-AC02-05CH11231 and the Handy and LIred computer clusters at the Stony Brook University Institute for Advanced Computational Science.

## APPENDIX A: ALTERNATIVE MATERIALS

In these appendices, we provide a few more details that are not essential for understanding the letter. In particular, we describe a few other scintillators that may be suitable target materials, describe the scintillation mechanisms of various materials mentioned in Table I of the main text and these alternative candidate materials, and give a brief discussion on whether the effect of excitons should be included in the calculation of the DM-electron scattering rates. For completeness, we also provide plots showing our calculated band structures and density of states for the five elements shown in Fig. 2, as well as the recoil spectra for GaAs, NaI, and CsI.

Other scintillator targets are possible, a select few of which we list in Table III. Plastic scintillators, e.g. PVT, have a low radiative efficiency, but this may be offset by their low production cost. $CaWO_4$ also has a low radiative efficiency [58]. Noble liquids can be scaled up relatively easily to large masses. At room temperature, phonons reduce radiative relaxation (i.e. quenching) in NaI and CsI, and $Tl^+$ doping is commonly used to provide efficient radiative centers. We include them to compare with the undoped cases. All listed materials (except PVT) are used for DM-nuclear recoil searches [21,27,31,59–68], but the photodetectors are not sensitive to single photons[5]

TABLE III. Band gap ($E_g$), radiative efficiency, photon emission energy peak ($E_{\rm em}^{\rm max}$), radiative recombination time ($\tau$), and scintillation mechanism ($Tl^+$ = thallium ion luminescent center, CX = charge-transfer emissions, excimers = short-lived, excited dimeric molecule) for candidate scintillators. In addition to the materials listed in Table I of the main text, other scintillators may also be suitable targets: polyvinyltoluene (PVT, i.e. $C_{27}H_{30}$), calcium tungstate ($CaWO_4$), xenon (Xe), argon (Ar), and helium (He). NaI and CsI, doped with thallium (NaI:Tl, CsI:Tl), scintillate at room temperature.

| Material | $E_g$ [eV] | Rad. Eff. | $E_{\rm em}^{\rm max}$ [eV] | $\tau$ [ns] | Mechanism |
|---|---|---|---|---|---|
| PVT [69] | 4.8 | 0.10 | 3.0 | 2 | organic |
| $CaWO_4$ [70] | 4.2 | 0.21 | 2.9 | 8000 | CX |
| Xe [71,72] | 12.1[a] | 0.30 | 7.1 | 30[b] | excimers |
| Ar [72,73] | 15.8[a] | 0.40 | 9.9 | $10^3$[b] | excimers |
| He [65] | 24.6[a] | 0.29 | 15.5 | 10[c] | excimers |
| NaI:Tl [74][d] | 5.9 | 0.50 | 3.0 | 115 | $Tl^+$ |
| CsI:Tl [74][d] | 6.4 | ∼1 | 2.2 | 980 | $Tl^+$ |

[a]Ionization energy of outer-shell electron [75].
[b]Triplet lifetime.
[c]Singlet lifetime.
[d]Room temperature values.

Other scintillator targets are possible, a select few of which we list in Table III. Plastic scintillators, e.g. PVT, have a low radiative efficiency, but this may be offset by their low production cost. $CaWO_4$ also has a low radiative efficiency [58]. Noble liquids can be scaled up relatively easily to large masses. At room temperature, phonons reduce radiative relaxation (i.e. quenching) in NaI and CsI, and $Tl^+$ doping is commonly used to provide efficient radiative centers. We include them to compare with the undoped cases. All listed materials (except PVT) are used for DM-nuclear recoil searches [21,27,31,59–68], but the photodetectors are not sensitive to single photons[5]

## APPENDIX B: BRIEF REVIEW OF SCINTILLATION MECHANISMS

We review briefly the scintillation mechanisms of the materials listed in Table I of the paper and Table III of these supplementary materials. In general, for a material to be a scintillator, it must contain luminescent centers. These centers can be either extrinsic (e.g. dopants and impurities) or intrinsic (e.g. defects of the lattice or excitons), and give rise to a transition between a higher- and a lower-energy state. Moreover, the energy levels involved in the transition must be contained in a forbidden energy region (e.g. the band gap for semiconductors and insulators, or excimer states in gases) to avoid re-absorption of the emitted light or photoionization of the center (Fig. 3).

Pure CsI and NaI at cryogenic temperatures scintillate via the formation of self-trapped excitons, where an exciton (an electron-hole bound state) becomes self-trapped by deforming the lattice structure around it. At cryogenic temperatures the system lies at the minimum energy in lattice configuration space, and the system can only return to the ground state by emission of a photon. At higher temperatures, thermally induced lattice vibrations allow the system to return to the ground state by phonon emission resulting in a low radiative efficiency. At room temperature, this thermal quenching is overcome by doping the material with e.g. thallium. In these cases, $Tl^+$ traps the excitons and provides an efficient luminescence center.

Direct-gap semiconductors, like GaAs, have the advantage that an excited electron can recombine with a hole without requiring a change in crystal momentum. In practice, however, dopants are used to enhance the radiative

[5]DM-electron scattering in e.g. xenon TPCs could produce two photons in a multistep deexcitation process. However the efficiency to detect a photon is low (e.g. ∼10% in LUX). Moreover, the PMTs are not sensitive to the second photon, which is in the infrared.

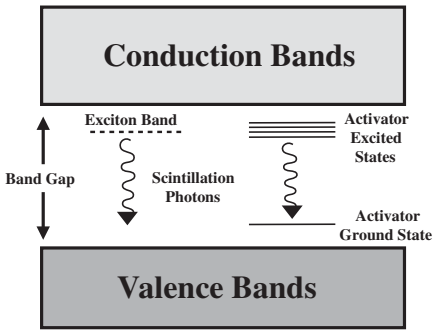


FIG. 3. Illustration of the different mechanisms for light emission in a scintillating crystal.

quantum efficiency, by providing radiative centers, and to reduce nonradiative recombination from impurities and native defects.

Indirect-gap semiconductors, like Si and Ge, require dopants to allow radiative recombination at cryogenic temperatures through the formation of a bound exciton that can radiate without the need for a change in crystal momentum.

Plastic scintillators consist of a base polymer that contains delocalized $\pi$-orbital electrons and a small concentration of fluorescent molecules. Excited $\pi$-orbital electrons will diffuse through the base polymer and excite fluorescent molecules. These excitations have radiative lifetimes of 1–2 nanoseconds. This process is efficient both at room and cryogenic temperatures.

In tungstate scintillators, valence-band electrons on the oxygen ions can be excited to conduction band states on the tungsten ions. In $PbWO_4$, the excited state is thermally quenched so that at room temperature the luminosity is low and the decay time is short. $CaWO_4$ and $CdWO_4$ are more efficient at room temperature and their decay times are $\sim$10 microseconds.

## APPENDIX C: EFFECT OF EXCITONS ON DARK MATTER-ELECTRON SCATTERING-RATE CALCULATION

Our calculation of the DM-electron scattering rate neglects the effect of *excitons*. In this section, we discuss why we expect this to be a good approximation for the low-band-gap materials (Ge, Si, and GaAs), but that there may be an $\mathcal{O}(1)$ correction for the large-band-gap insulators (NaI and CsI).

Semiconductors or insulating crystals are characterized by a finite band gap, $E_g$, between the top of the valence band and the bottom of the conduction band. These bands form an energy continuum for the excitation of an electron from the valence to the conduction band, which can be viewed as the creation of a free-electron-free-hole pair. In our calculation of the DM-electron scattering rate, we included the contribution of this continuum of states.

The small electrostatic Coulomb attraction between the negatively charged electron and positively charged hole creates an exciton, a bound electron-hole pair (see e.g. [76–79] and references therein). As we will see below, this Coulomb-bound electron-hole pair can be modeled with Rydberg-like states with energies $E_g - E_{B,n}$, where $E_{B,n}$ is the binding energy and $n$ labels the Rydberg-like energy level. The energy of these excitons is therefore in the "forbidden" band-gap region, so that the density of states is nonzero even at energies slightly below the conduction band. Moreover, the bound electron-hole pair has ionized states with a continuous energy due to their relative motion. It turns out that excitons therefore also moderately increase the density of states just below the band gap compared to a calculation that neglects them. Including exciton effects in the DM-electron scattering-rate calculation could thus be important for two reasons. First, a nonzero density of states below the band gap means that the actual mass threshold is slightly lower. Second, any calculation that neglects exciton effects might underestimate slightly the scattering rate.

Excitons are extensively studied in solid state physics and play an important role in determining the properties of various materials. For example, it is well known that excitons are crucial in understanding the spectrum for the absorption of light, as they allow for photons with an energy just below $E_g$ to be absorbed by an electron. Similarly, excitons can play an essential role in determining the scintillation properties of a material. For example, an electron excited from the valence to the conduction band can quickly relax to the bottom of the conduction band and then into an exciton state by emitting phonons. The radiative decay of the exciton then yields a photon whose energy is just below that of the band gap. This typically allows the photon to traverse the material without being absorbed again, i.e. the material scintillates.

We can estimate how far below the conduction band the density of states will be nonzero from exciton effects by using a hydrogen-like model for the electron-hole pair. In particular, the exciton binding energies $E_{B,n}$ can be approximated by a modified Rydberg energy, namely

$$\Delta E_{B,n} = \frac{\alpha^2 \mu_{eh}}{2\varepsilon^2 n^2}, \tag{C1}$$

where $\varepsilon$ is the dielectric constant of the crystal, $n = 1, 2, \ldots$, and $\mu_{eh}$ is the effective electron-hole reduced mass, given by

$$\mu_{eh}^* = \left(\frac{1}{m_e^*} + \frac{1}{m_h^*}\right)^{-1}, \tag{C2}$$

TABLE IV. Dielectric constant ($\varepsilon$), effective electron mass ($m_e^*$), effective hole mass ($m_h^*$), 1s-exciton binding energy, and 1s-exciton radius (in units of the lattice constant $a$ in Table II of main text) for various materials.

| | $\varepsilon$ | $m_e^*/m_e$ | $m_h^*/m_e$ | $\Delta E_{B,n=1}$ [eV] | $a_{n=1}/a$ |
|---|---|---|---|---|---|
| CsI [80,81] | 5.65 | 0.312 | 2.270 | 0.117 | 2.37 |
| NaI [81,82] | 7.28 | 0.287 | 2.397 | 0.066 | 2.20 |
| GaAs [80,83] | 12.85 | 0.067 | 0.45 | 0.005 | 20.3 |
| Ge [80,83] | 16 | 0.2 | 0.28 | 0.006 | 12.7 |
| Si [80,83] | 13 | 0.33 | 0.49 | 0.016 | 6.38 |

where $m_e^*$ ($m_h^*$) is the effective electron (hole) mass. In this approximation, the electron-hole pair is assumed to be subject to a screened Coulomb potential characterized by the dielectric constant $\varepsilon$. This is a good approximation only if the exciton radius, $a_n$, is much larger than the lattice constant (*Wannier* exciton). The exciton radius is given by

$$a_n = \frac{\varepsilon m_e n^2}{\mu_{eh}} a_0, \tag{C3}$$

where $a_0$ is the (hydrogen) Bohr radius. The relevant values for the materials we considered in the letter are given in Table IV, which also lists the binding energy and size of the various 1s exciton states (i.e. with $n = 1$).

The 1s-exciton radii listed in Table III for GaAs, Ge, and Si are much larger than the lattice constants given in Table II, so that the approximation of the binding energies with Eq. (8) is expected to be reasonable. For NaI and CsI, the approximation is expected to be worse, but not dramatically so. We can thus use this simple estimate of the binding energies to reach at least qualitative conclusions for how the inclusion of exciton effects might affect the DM-mass threshold and the DM-electron scattering-rate calculation.

First, we see from Table III that the 1s-exciton binding energies for the low-band-gap materials, GaAs, Ge, and Si, are very small, ∼10 meV, but even for the insulators, NaI and CsI, the binding energy only reaches about ∼100 meV. This lowers the mass threshold by ∼1–30 keV, depending on the material, an effect that is smaller than the numerical uncertainty of the rate calculation without excitons.

Second, recall that the electron's recoil energy after a DM scattering event is typically several eV. The typical recoil energy is thus larger than the band gap energy for semiconductors like GaAs, Ge, and Si. A moderate increase in the density of states from the inclusion of exciton effects 10 meV below the band gap, as well as just above it, is thus not expected to be important in the rate calculation. For the insulators NaI and CsI with band gaps around 6 eV, an increase in the density of states below and above the conduction band's bottom could be somewhat important, since the electron will largely prefer to scatter to those states rather than higher-energy ones.

The calculation of exciton effects in the DM-electron scattering requires a dedicated effort. One reason for this is that existing numerical codes usually calculate exciton effects for photon absorption or emission. However, a photon being absorbed by an electron does not significantly change the momentum of the electron, so that the transition from valence to conduction band occurs at roughly the same $k$-point. Instead, DM scattering off an electron does transfer a sizable momentum, comparable with the crystal momentum.

The above discussion shows that it would be desirable to include exciton effects for NaI and CsI in the future. Neglecting the exciton effects, as we have done in our calculations, gives an overall conservative estimate for the DM-electron scattering rates.

## APPENDIX D: RECOIL SPECTRA FOR GALLIUM ARSENIDE, SODIUM IODIDE, AND CESIUM IODIDE

Figure 4 shows the electron recoil spectra from DM-electron scattering for GaAs, NaI, and CsI. as a function of total deposited energy $E_e$, for two DM masses and two choices for the DM form factor. We include also spectra for Ge and Si for comparison (see also [2]). As expected, the spectra extend to higher recoil energies for higher DM masses, and $F_{\rm DM} \propto 1/q^2$ spectra decrease faster than those for $F_{\rm DM} = 1$, since lower momentum transfers are preferred. Bump-like features in the spectra are explained by comparing the energy at which they occur with the energies of the available valence bands.

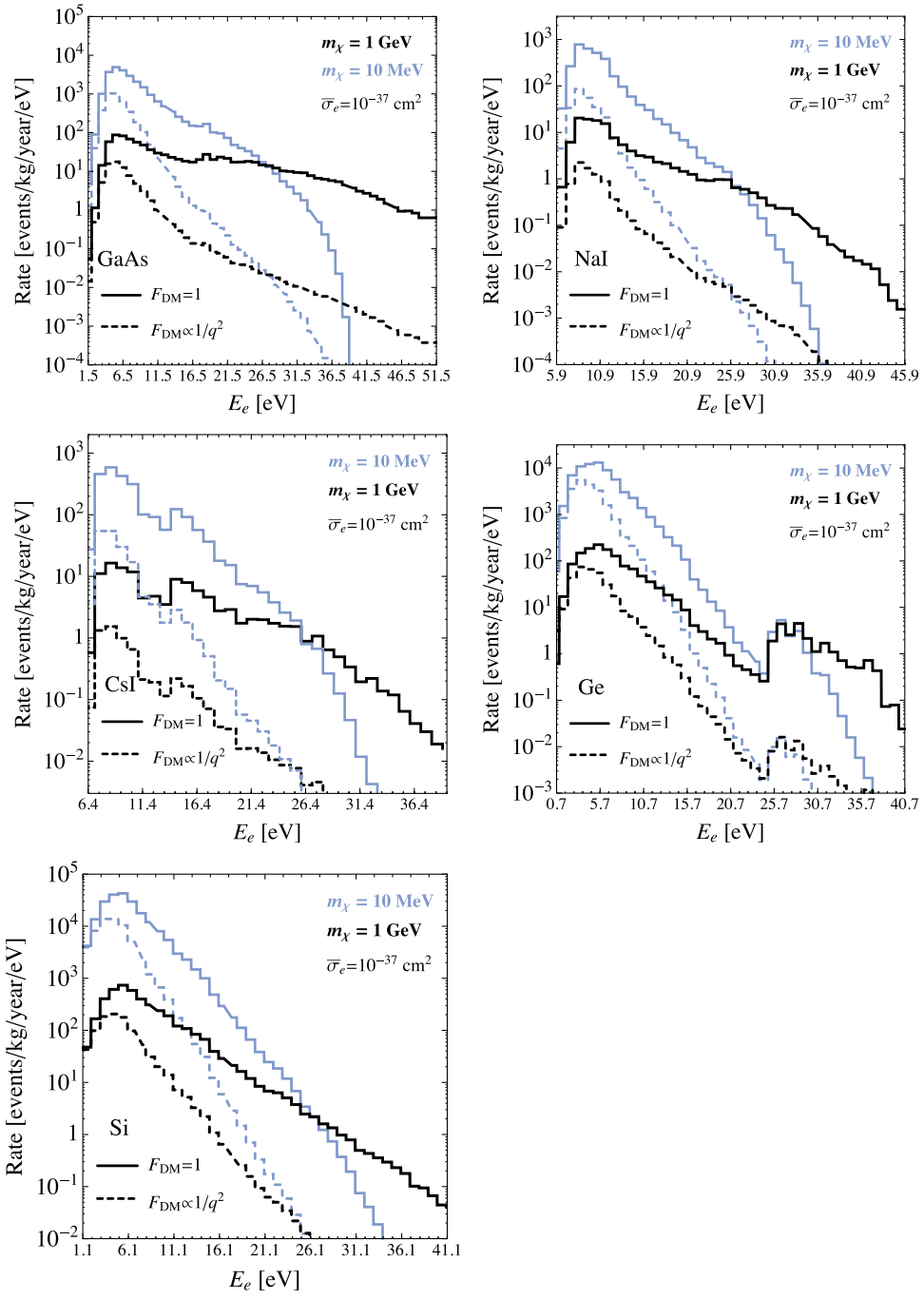


FIG. 4. Electron recoil spectra from DM-electron scattering in GaAs, NaI, CsI, Ge, and Si as a function of total deposited energy $E_e$, for $m_\chi = 10$ MeV (blue lines) and 1 GeV (black lines) and DM form factors $F_{\rm DM} = 1$ (solid lines) and $F_{\rm DM} = (\alpha m_e/q)^2$ (dashed lines). We fix $\bar{\sigma}_e = 10^{-37}$ cm$^2$ and assume an exposure of 1 kg-year. The $E_e$-axis begins at the band-gap energies $E_g$.

## APPENDIX E: DENSITY OF STATES AND BAND STRUCTURES

Figure 5 shows our calculated band structure and density of states (DoS) for GaAs, NaI, and CsI. For completeness, we include slightly modified plots from [2] for Ge and Si. We show all valence electron levels included in our DM-electron-scattering-rate calculation as well as the bottom of the conduction band.

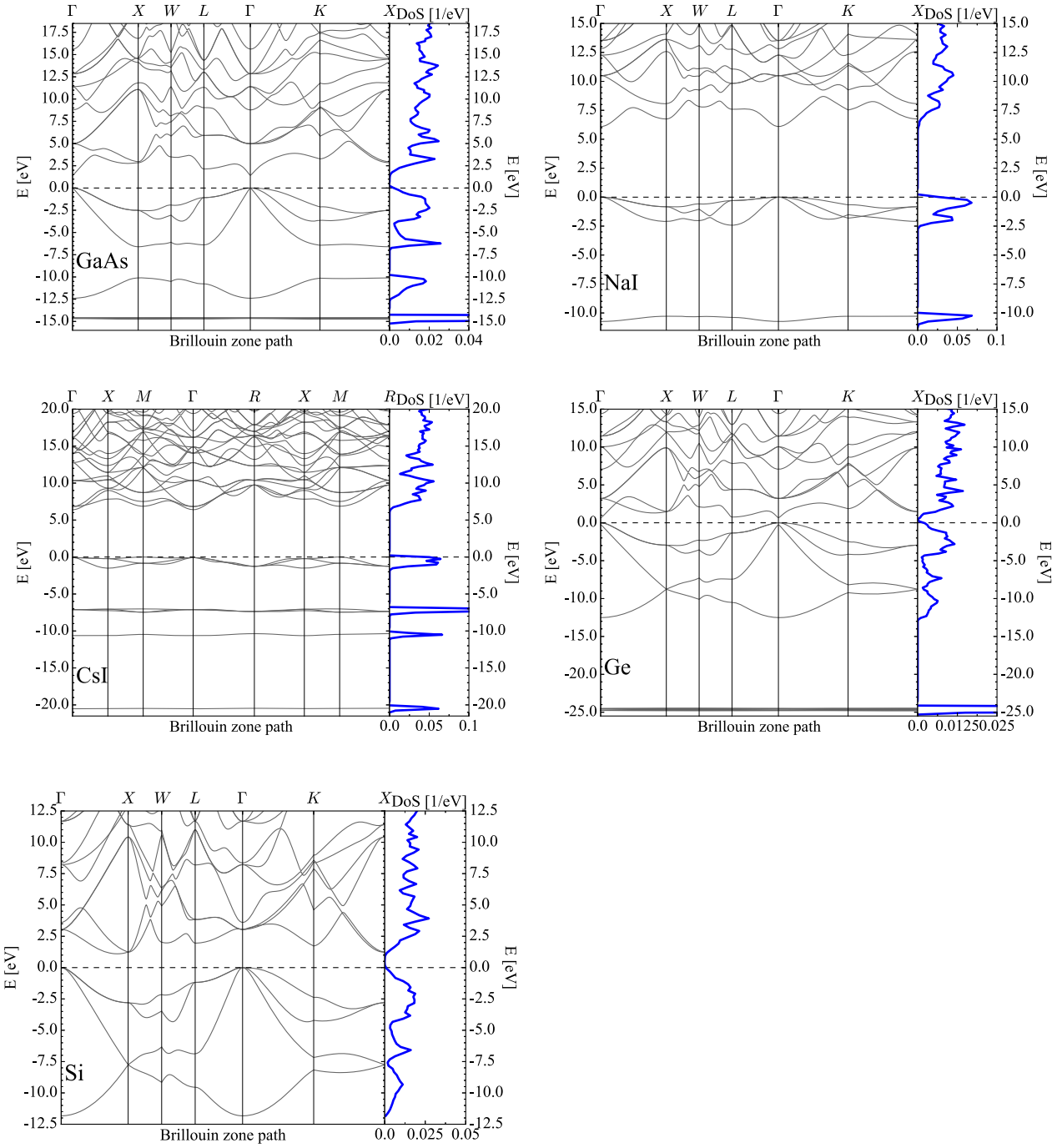


FIG. 5. Calculated band structure (black lines) and density of states (DoS, blue lines) of the electronic states for gallium arsenide (GaAs), sodium iodide (NaI), cesium iodide (CsI), germanium (Ge), and silicon (Si). We show all valence electron states included in our DM-electron-scattering-rate calculation as well as the bottom of the conduction band. The DoS was calculated by smearing the energy with a Gaussian function of width $\delta E = 0.25$ eV.

[1] R. Essig, J. Mardon, and T. Volansky, Phys. Rev. D **85**, 076007 (2012).

[2] R. Essig, M. Fernandez-Serra, J. Mardon, A. Soto, T. Volansky, and T.-T. Yu, J. High Energy Phys. 05 (2016) 046.

[3] P. W. Graham, D. E. Kaplan, S. Rajendran, and M. T. Walters, Phys. Dark Universe **1**, 32 (2012).

[4] S. K. Lee, M. Lisanti, S. Mishra-Sharma, and B. R. Safdi, Phys. Rev. D **92**, 083517 (2015).

[5] R. Essig, A. Manalaysay, J. Mardon, P. Sorensen, and T. Volansky, Phys. Rev. Lett. **109**, 021301 (2012).

[6] Y. Hochberg, Y. Zhao, and K. M. Zurek, Phys. Rev. Lett. **116**, 011301 (2016); Y. Hochberg, M. Pyle, Y. Zhao, and K. M. Zurek, J. High Energy Phys. 08 (2016) 057; K. Schutz and K. M. Zurek, Phys. Rev. Lett. **117**, 121302 (2016); Y. Hochberg, Y. Kahn, M. Lisanti, C. G. Tully, and K. M. Zurek, Phys. Lett. B **772**, 239 (2017).

[7] R. Essig, J. A. Jaros, W. Wester, P. H. Adrian, S. Andreas *et al.*, arXiv:1311.0029; C. Bird, P. Jackson, R. V. Kowalewski, and M. Pospelov, Phys. Rev. Lett. **93**, 201803 (2004); N. Borodatchenkova, D. Choudhury, and M. Drees, Phys. Rev. Lett. **96**, 141802 (2006); B. McElrath, Phys. Rev. D **72**, 103508 (2005); P. Fayet, Phys. Rev. D **74**, 054034 (2006); C. Bird, R. V. Kowalewski, and M. Pospelov, Mod. Phys. Lett. A **21**, 457 (2006); Y. Kahn, M. Schmitt, and T. M. Tait, Phys. Rev. D **78**, 115002 (2008); P. Fayet, Phys. Rev. D **75**, 115017 (2007); R. Essig, P. Schuster, and N. Toro, Phys. Rev. D **80**, 015003 (2009); J. D. Bjorken, R. Essig, P. Schuster, and N. Toro, Phys. Rev. D **80**, 075018 (2009); M. Reece and L.-T. Wang, J. High Energy Phys. 07 (2009) 051; P. Fayet, Phys. Rev. D **81**, 054025 (2010); G. K. Yeghiyan, Phys. Rev. D **80**, 115019 (2009); A. Badin and A. A. Petrov, Phys. Rev. D **82**, 034005 (2010); B. Echenard, Mod. Phys. Lett. A **27**, 1230016 (2012); J. March-Russell, J. Unwin, and S. M. West, J. High Energy Phys. 08 (2012) 029; R. Essig, J. Mardon, M. Papucci, T. Volansky, and Y.-M. Zhong, J. High Energy Phys. 11 (2013) 167; R. Essig, E. Kuflik, S. D. McDermott, T. Volansky, and K. M. Zurek, J. High Energy Phys. 11 (2013) 193; C. Boehm, M. J. Dolan, and C. McCabe, J. Cosmol. Astropart. Phys. 08 (2013) 041; K. M. Nollett and G. Steigman, Phys. Rev. D **89**, 083508 (2014); S. Andreas *et al.*, Phys. Rev. D **89**, 075008 (2014); E. Izaguirre, G. Krnjaic, P. Schuster, and N. Toro, Phys. Rev. D **88**, 114015 (2013); M. Battaglieri *et al.* (BDX Collaboration), arXiv:1406.3028; E. Izaguirre, G. Krnjaic, P. Schuster, and N. Toro, Phys. Rev. D **91**, 094026 (2015); B. Batell, R. Essig, and Z. Surujon, Phys. Rev. Lett. **113**, 171802 (2014); Y. Kahn, G. Krnjaic, J. Thaler, and M. Toups, Phys. Rev. D **91**, 055006 (2015); G. Krnjaic, Phys. Rev. D **94**, 073009 (2016); B. Batell, M. Pospelov, and A. Ritz, Phys. Rev. D **80**, 095024 (2009); E. Izaguirre, G. Krnjaic, P. Schuster, and N. Toro, Phys. Rev. Lett. **115**, 251301 (2015).

[8] C. Boehm and P. Fayet, Nucl. Phys. **B683**, 219 (2004); M. J. Strassler and K. M. Zurek, Phys. Lett. B **651**, 374 (2007); N. Arkani-Hamed, D. P. Finkbeiner, T. R. Slatyer, and N. Weiner, Phys. Rev. D **79**, 015014 (2009); M. Pospelov and A. Ritz, Phys. Lett. B **671**, 391 (2009); D. Hooper and K. M. Zurek, Phys. Rev. D **77**, 087302 (2008); J. L. Feng and J. Kumar, Phys. Rev. Lett. **101**, 231301 (2008); D. E. Morrissey, D. Poland, and K. M. Zurek, J. High Energy Phys. 07 (2009) 050; R. Essig, J. Kaplan, P. Schuster, and N. Toro, arXiv:1004.0691; T. Cohen, D. J. Phalen, A. Pierce, and K. M. Zurek, Phys. Rev. D **82**, 056001 (2010); T. Lin, H.-B. Yu, and K. M. Zurek, Phys. Rev. D **85**, 063503 (2012); X. Chu, T. Hambye, and M. H. Tytgat, J. Cosmol. Astropart. Phys. 05 (2012) 034; Y. Hochberg, E. Kuflik, T. Volansky, and J. G. Wacker, Phys. Rev. Lett. **113**, 171301 (2014); Y. Hochberg, E. Kuflik, H. Murayama, T. Volansky, and J. G. Wacker, Phys. Rev. Lett. **115**, 021301 (2015).

[9] P. Cushman *et al.*, in *Community Summer Study 2013: Snowmass on the Mississippi (CSS2013) Minneapolis, MN, USA, July 29-August 6, 2013* (2013) [arXiv:1310.8327].

[10] J. Angle *et al.* (XENON10 Collaboration), Phys. Rev. Lett. **107**, 051301 (2011); **110**, 249901(E) (2013).

[11] R. Agnese *et al.* (SuperCDMS Collaboration), Phys. Rev. Lett. **116**, 071301 (2016).

[12] G. Fernandez Moroni, J. Estrada, G. Cancelo, S. E. Holland, E. E. Paolini, and H. T. Diehl, Exp. Astron. **34**, 43 (2012).

[13] G. D. Starkman and D. N. Spergel, Phys. Rev. Lett. **74**, 2623 (1995).

[14] B. A. Mazin, B. Bumble, S. R. Meeker, K. O'Brien, S. McHugh, and E. Langman, Opt. Express **20**, 1503 (2012).

[15] K. Irwin and G. Hilton, Top. Appl. Phys. **99**, 63 (2005).

[16] M. D. Petroff, M. G. Stapelbroek, and W. A. Kleinhans, Appl. Phys. Lett. **51**, 406 (1987).

[17] D. F. Santavicca, B. Reulet, B. S. Karasik, S. V. Pereverzev, D. Olaya, M. E. Gershenson, L. Frunzio, and D. E. Prober, Appl. Phys. Lett. **96**, 083505 (2010).

[18] B. S. Karasik, S. V. Pereverzev, A. Soibel, D. F. Santavicca, D. E. Prober, D. Olaya, and M. E. Gershenson, Appl. Phys. Lett. **101**, 052601 (2012).

[19] D. J. Goldie, A. V. Velichko, D. M. Glowacka, and S. Withington, J. Appl. Phys. **109**, 084507 (2011).

[20] A. J. Miller, S. W. Nam, J. M. Martinis, and A. V. Sergienko, Appl. Phys. Lett. **83**, 791 (2003).

[21] G. Angloher *et al.* (CRESST Collaboration), Eur. Phys. J. C **76**, 25 (2016).

[22] G. Angloher *et al.*, Astropart. Phys. **84**, 70 (2016).

[23] M. Pyle, *U.S. Cosmic Visions 2017, University of Maryland*.

[24] M. Biroth, P. Achenbach, E. Downie, and A. Thomas, Nucl. Instrum. Methods Phys. Res., Sect. A **787**, 68 (2015).

[25] P. Achenbach, M. Biroth, E. Downie, and A. Thomas, Nucl. Instrum. Methods Phys. Res., Sect. A **824**, 74 (2016).

[26] J. Liu, M. Yamashita, and A. K. Soma, J. Instrum. **11**, P10003 (2016).

[27] E. Aprile *et al.* (XENON100 Collaboration), Phys. Rev. D **94**, 092001 (2016).

[28] P. Luke, J. Beeman, F. Goulding, S. Labov, and E. Silver, Nucl. Instrum. Methods Phys. Res., Sect. A **289**, 406 (1990).

[29] B. Neganov and V. Trofimov, Otkrytiya, Izobret **146**, 215 (1985).

[30] R. Agnese *et al.* (SuperCDMS Collaboration), Phys. Rev. D **95**, 082002 (2017).

[31] F. Froborg (SABRE Collaboration), J. Phys. Conf. Ser. **718**, 042021 (2016).

[32] Y. S. Yoon *et al.* (KIMS Collaboration), J. High Energy Phys. 06 (2016) 011.

[33] N. Abgrall *et al.* (Majorana Collaboration), Phys. Rev. Lett. **118**, 161801 (2017).

[34] A. K. Drukier, K. Freese, and D. N. Spergel, Phys. Rev. D **33**, 3495 (1986).
[35] D. Tucker-Smith and N. Weiner, Phys. Rev. D **64**, 043502 (2001).
[36] M. Moszynski, M. Balcerzyk, W. Czarnacki, M. Kapusta, W. Klamra, P. Schotanus, A. Syntfeld, and M. Szawlowski, IEEE Trans. Nucl. Sci. **50**, 767 (2003).
[37] M. Moszynski, M. Balcerzyk, W. Czarnacki, M. Kapusta, W. Klamra, P. Schotanus, A. Syntfeld, M. Szawlowski, and V. Kozlov, Nucl. Instrum. Methods Phys. Res., Sect. A **537**, 357 (2005).
[38] C. Amsler, D. Grgler, W. Joffrain, D. Lindelf, M. Marchesotti, P. Niederberger, H. Pruys, C. Regenfus, P. Riedler, and A. Rotondi, Nucl. Instrum. Methods Phys. Res., Sect. A **480**, 494 (2002).
[39] D. Cusano, Solid State Commun. **2**, 353 (1964).
[40] *Applied Gamma-Ray Spectrometry*, 2nd ed. completely revised and enlarged, edited by C. C. Adams and R. Dams, International Series of Monographs on Analytical Chemistry (Pergamon, New York, 1970), Vol. 2, p. iv.
[41] R. Hofstadter, Phys. Rev. **75**, 796 (1949).
[42] R. Hofstadter, Phys. Rev. **75**, 1611 (1949).
[43] http://www.crystals.saint-gobain.com/, accessed: 2016-02-17.
[44] M. Moszyriski, A. Nassalski, A. Syntfeld-Kazuch, L. Swiderski, and T. Szczesniak, IEEE Trans. Nucl. Sci. **55**, 1062 (2008).
[45] C. Sailer, B. Lubsandorzhiev, C. Strandhagen, and J. Jochum, Eur. Phys. J. C **72**, 2061 (2012).
[46] V. B. Mikhailik, V. Kapustyanyk, V. Tsybulskyi, V. Rudyk, and H. Kraus, Phys. Status Solidi B **252**, 804 (2015).
[47] A. Knapitsch and P. Lecoq, Int. J. Mod. Phys. A **29**, 1430070 (2014).
[48] S. E. Derenzo, E. Bourret-Courchesne, F. J. James, M. K. Klintenberg, Y. Porter-Chapman, J. Wang, and M. J. Weber, IEEE Nuclear Science Symposium Conference Record **2**, 1132 (2006).
[49] M. Steger, A. Yang, T. Sekiguchi, K. Saeedi, M. L. W. Thewalt, M. O. Henry, K. Johnston, H. Riemann, N. V. Abrosimov, M. F. Churbanov, A. V. Gusev, A. K. Kaliteevskii, O. N. Godisov, P. Becker, and H.-J. Pohl, J. Appl. Phys. **110**, 081301 (2011).
[50] G. Davies, Phys. Scr. **T54**, 7 (1994).
[51] G. Davies, E. C. Lightowlers, K. Itoh, W. L. Hansen, E. E. Haller, and V. Ozhogin, Semicond. Sci. Technol. **7**, 1271 (1992).
[52] J. P. Perdew, K. Burke, and M. Ernzerhof, Phys. Rev. Lett. **77**, 3865 (1996).
[53] D. R. Hamann, M. Schlüter, and C. Chiang, Phys. Rev. Lett. **43**, 1494 (1979).
[54] Z. Levine and D. Allan, Phys. Rev. Lett. **63**, 1719 (1989).
[55] Z. Levine and D. Allan, Phys. Rev. B **43**, 4187 (1991).
[56] C. A. Klein, J. Appl. Phys. **39**, 2029 (1968).
[57] G. F. Knoll, *Radiation Detection and Measurement*, 4th ed. (Wiley, New York, NY, 2010).
[58] M. Moszynski, M. Balcerzyk, W. Czarnacki, A. Nassalski, T. Szczesniak, H. Kraus, V. B. Mikhailik, and I. M. Solskii, Nucl. Instrum. Methods Phys. Res., Sect. A **553**, 578 (2005).
[59] G. Angloher, M. Bauer, I. Bavykina, A. Bento, A. Brown, C. Bucci, C. Ciemniak, C. Coppi, G. Deuter, and F. von Feilitzsch, Astropart. Phys. **31**, 270 (2009).
[60] D. S. Akerib *et al.* (LUX Collaboration), Phys. Rev. Lett. **116**, 161302 (2016).
[61] K. Abe *et al.*, Nucl. Instrum. Methods Phys. Res., Sect. A **716**, 78 (2013).
[62] E. Aprile *et al.* (XENON Collaboration), J. Cosmol. Astropart. Phys. 04 (2016) 027.
[63] D. S. Akerib *et al.* (LZ Collaboration), arXiv:1509.02910.
[64] C. E. Aalseth *et al.*, Adv. High Energy Phys. **2015**, 541362 (2015).
[65] W. Guo and D. N. McKinsey, Phys. Rev. D **87**, 115001 (2013).
[66] R. Bernabei *et al.* (DAMA, LIBRA Collaboration), Eur. Phys. J. C **67**, 39 (2010).
[67] E. Barbosa de Souza *et al.* (DM-Ice Collaboration), Phys. Rev. D **95**, 032006 (2017).
[68] H. S. Lee *et al.* (KIMS Collaboration), Phys. Rev. Lett. **99**, 091301 (2007).
[69] G. Trilling, *Bubble Chamber Physics in the Seventies* (Lawrence Radiation Laboratory, Berkeley, California, 1970).
[70] Y. Zdesenko, F. A. III, V. Brudanin, F. Danevich, S. Nagorny, I. Solsky, and V. Tretyak, Nucl. Instrum. Methods Phys. Res., Sect. A **538**, 657 (2005).
[71] E. Aprile, L. Baudis, B. Choi, K. L. Giboni, K. Lim, A. Manalaysay, M. E. Monzani, G. Plante, R. Santorelli, and M. Yamashita, Phys. Rev. C **79**, 045807 (2009).
[72] V. Chepel and H. Araujo, J. Instrum. **8**, R04001 (2013).
[73] P. M. Dehmer and S. T. Pratt, J. Chem. Phys. **76**, 843 (1982).
[74] J. T. M. de Haas and P. Dorenbos, IEEE Trans. Nucl. Sci. **55**, 1086 (2008).
[75] J. E. Sansonetti, W. C. Martin, and S. L. Young, *Handbook of Basic Atomic Spectroscopic Data (version 1.1.3)* (National Institute of Standards and Technology, Gaithersburg, 2005).
[76] R. Knox, *Theory of excitons*, Solid state physics: Supplement (Academic Press, New York, 1963).
[77] A. Song and R. Williams, *Self-trapped excitons*, Springer series in solid-state sciences (Springer, New York, 1996).
[78] K. Cho, P. Dean, B. Fischer, D. Herbert, J. Lagois, and P. Yu, *Excitons*, Topics in Current Physics (Springer, Berlin Heidelberg, 2012).
[79] R. Kubo and E. Hanamura, *Springer Series in Solid-State Sciences* (Springer, Berlin Heidelberg, 2012).
[80] http://www.almazoptics.com, accessed: 2016-06-16.
[81] W. Setyawan, R. M. Gaume, R. S. Feigelson, and S. Curtarolo, IEEE Trans. Nucl. Sci. **56**, 2989 (2009).
[82] K. Kamiyoshi and Y. Nigara, Phys. Status Solidi (a) **3**, 735 (1970).
[83] J. Singh, *Physics of Semiconductors and Their Heterostructures* (McGraw-Hill, New York, 1992).